Article

New *Quantum*-Dot-Based Fluorescent Immunosensor for Cancer Biomarker Detection

Mariana P. Sousa [1,2,3,4], Ana Margarida L. Piloto [1,2], Ana Cláudia Pereira [3], Fernando C. Schmitt [4,5,6], Ruben Fernandes [3,5,7] and Felismina T. C. Moreira [1,2,*]

1   BioMark/ISEP, School of Engineering, Polytechnic of Porto, 4200-072 Porto, Portugal
2   CEB—Centre of Biological Engineering, University of Minho, 4710-057 Braga, Portugal
3   Laboratory of Medical and Industrial Biotechnology (LaBMI), Porto Research, Technology and Innovation Center (PORTIC), Porto Polytechnic Institute, 4785-999 Porto, Portugal
4   Faculty of Medicine, University of Porto, 4200-319 Porto, Portugal
5   CINTESIS@RISE, Health Research Network, 4200-319 Porto, Portugal
6   IPATIMUP—Institute of Molecular Pathology and Immunology of University of Porto, 4200-135 Porto, Portugal
7   FP-I3ID, FP-BHS, Faculty of Health Sciences, Hospital Fernando Pessoa, University Fernando Pessoa, 4200-150 Porto, Portugal
*   Correspondence: ftm@isep.ipp.pt

Abstract: Cancer antigen 15-3 (CA 15-3) is a biomarker for breast cancer used to monitor response to treatments and disease recurrence. The present work demonstrates the preparation and application of a fluorescent biosensor for ultrasensitive detection of the cancer antigen CA 15-3 protein tumor marker using mercaptopropionic-acid-functionalized cadmium telluride (CdTe@MPA) *quantum* dots (QDs) conjugated with CA 15-3 antibodies. First, the QDs were synthesized by the hydrothermal route, resulting in spherical nanoparticles up to 3.50 nm in diameter. Subsequently, the QD conjugates were characterized by Fourier transform infrared spectroscopy (FTIR), UV absorption, and fluorescence. The interaction between the conjugates and the protein was studied by fluorescence spectroscopy in buffer and in 10-fold diluted commercial human serum. Calibration in spiked serum samples gave a detection limit of 0.027 U/mL, 1000-fold lower than the clinical limit for CA 15-3 (25 U/mL to 30 U/mL), indicating that this is an ultrasensitive technique. In addition, a rapid response was obtained within 10 min. The biosensor was selective in the presence of the interfering serum proteins BSA, CEA, and CA-125, with a maximum interference of 2% for BSA. The percent recovery was close to 100% with maximum relative standard deviation (RSD%) values of 1.56. Overall, the developed CA 15-3 biosensor provides a simple and sensitive method for ultrasensitive monitoring of breast cancer, as well as the ability to detect other molecules of interest in human serum matrices.

Keywords: antibody; CA 15-3 biosensor; fluorescence; quantum dot

1. Introduction

Over the last few years, *quantum* dots (QDs) have been extensively studied for a wide variety of applications from medicine to optoelectronics [1,2]. A variety of QDs have been reported. In general, QDs are binary, i.e., they are composed of elements from the groups II–VI, but they can also be fabricated from single elements, namely silicon or germanium [3,4]. In recent years, active research in this field has led to the synthesis of QDs using transition metals, chalcogenic elements, and carbon, among others [1,5].

Due to their high brightness, large molar extinction coefficient, photostability, and tunable wavelength, QDs represent an advantageous alternative to conventional fluorophores, such as organic dyes or proteins [6–8]. The biocompatibility of carbon and graphene QDs has been demonstrated for bioimaging, photodynamic therapy, and drug delivery both in vitro and in vivo [8,9]. Moreover, the surface of QDs can be easily modified with recognition molecules such as antibodies, peptides, or aptamers, which extends their applicability

in the biomedical applications for sensitive and specific approaches to diagnostic and biosensing devices [8]. Among the various QDs, cadmium telluride (CdTe) nanoparticles have been particularly studied for these applications due to their high stability, tunable photoluminescence in the visible range, and high *quantum* yield [10,11]. Biosensing devices employing CdTe nanoparticles to track microbes such as bacteria [12,13] or viruses [14], glucose levels [15], or even cardiovascular diseases [16] have already been described in the literature.

Cancer incidence remains a significant burden in our society. By 2040, 29 million new cases are expected to be diagnosed worldwide. Among them, breast cancer is the most-common cancer, with more than 2.26 million cases diagnosed in 2020 (WHO, 2020) [17].

In addition to traditional screening methods, namely mammography and ultrasound, blood tests provide valuable information, especially by measuring biomarkers of breast cancer [18]. Biomarkers can be categorized based on their clinical information: risk assessment biomolecules, such as the BRCA1/2 and TP53 genes, help assess cancer risk; molecules for subtyping breast cancer and predicting response to treatment, which include hormone receptors and the HER2 protein; prognosis and disease progression by measuring proteins such as carcinoembryonic antigen (CEA) or CA 15-3 [18,19].

Although standard methods for measuring biomarkers, such as ELISA assays, LC/MS, or HPLC, provide sensitive and specific results, these technologies are time consuming and expensive [20,21]. In this way, biosensors are gaining interest due to their rapid, affordable, and point-of-care (PoC) characteristics [22].

The CA15-3 protein is commonly used as a serum biomarker for monitoring breast cancer treatment and recurrence. Its normal serum value is below 30 U/mL, and its increase is associated with the development of metastases [23]. For this reason, monitoring the CA 15-3 level is of clinical value in assessing disease progression and treatment efficacy.

Despite their high sensitivity and specificity, conventional techniques such as ELISA, electrochemiluminescence, or mass spectrometry are time consuming and require skilled laboratory personnel to be performed, resulting in high costs for healthcare systems and the general population [24].

To overcome this, several biosensors targeting the protein CA 15-3 have been described. Among all of them, electrochemical sensors provide the highest sensitivity with the lowest detection limit of up to 5×10^{-6} U/mL [25]. The use of nanomaterials, due to their catalytic properties, is often employed to improve the sensitivity of the devices into which they are inserted. Overall, the devices differ mainly in the type of electrode, electrochemical technique, and sensing platform [26]. Despite their high sensitivity and selectivity, electrochemical approaches are complex and lead to more expensive devices. Therefore, optical sensors are gaining interest because they are affordable and faster while maintaining the high specificity of electrochemical devices [27]. Optical methods for CA 15-3 detection range from photoluminescence to Förster or fluorescence resonance energy transfer (FRET), surface plasmon resonance, fluorescence, and colorimetric approaches [26,28] with the lowest detection limit of 50×10^{-6} U/mL. Although the sensor has high specificity and sensitivity, the use of molecularly imprinted polymers modified with nanomaterials leads to complex, multistep production associated with increased costs [28].

In this paper, we report a simple and inexpensive QD-based immunosensor designed to monitor CA 15-3 levels in human serum. For this purpose, (i) CdTe QDs were synthesized by hydrothermal methods and characterized by UV–Vis absorption, Fourier transform infrared spectroscopy (FTIR), scanning electron microscopy (SEM), energy dispersive X-ray spectroscopy (EDS), and fluorescence spectroscopy. (ii) The nanoparticles were then directly conjugated to the monoclonal antibody CA 15-3 and further characterized using the same techniques. (iii) The performance of the sensor was evaluated by fluorescence spectroscopy in spiked saline buffer and commercial human serum. The device has a detection limit of 0.027 U/mL and gives a response within 10 min.

2. Materials and Methods

2.1. Chemicals and Solutions

All chemicals used were of analytical research grade. Cadmium chloride monohydrated 99.99% was acquired from Acros Organics, (Geel, Belgium); tellurium powder 99.99% was acquired from Sigma Aldrich, (San Luis, MO, USA); 3-mercaptopropionic acid (MPA) was purchased from Sigma Aldrich; sodium borohydride was acquired from VWR; phosphate-buffered saline (PBS) was obtained from Fisher BioReagents, (Waltham, MA, USA); glycine was purchased from Merck, (Darmstadt, Germany); N-(3-dimethylaminopropyl)-N′-ethylcarbodiimide hydrochloride (EDAC) was obtained from Sigma Aldrich; N-hydroxysuccinimide (NHS) was acquired from Merck; mouse monoclonal mucin1 antibody (Vu-2G7) was purchased from Santa Cruz Biotechnology, (Dallas, TX, USA); the CA 15-3 protein was acquired from Emelca BioScience, (Antwerpen, Belgium); human serum HN was purchased from PZ CORMAY S.A., (Lomianki, Poland). Deionized water (conductivity < 0.1 µS/cm) was obtained from a Millipore water purification system and used throughout the experiment.

2.2. Apparatus

Both the QD nanoparticles and the corresponding conjugates were characterized by FTIR spectroscopy, SEM, absorption spectroscopy, and fluorescence spectroscopy.

FTIR spectroscopy was performed using a Nicolet iS100 (Thermo Scientific, Waltham, MA, USA) spectrometer coupled to an attenuated total reflectance (ATR) sensor with diamond contact crystal. Both sample and background spectra were acquired under the control of room temperature and humidity with 80 scans and a resolution of 8 cm^{-1} in the spectral range from 530 to 4000 cm^{-1}. The surface morphology of the red-emitting QDs was studied using a field emission scanning electron microscope (FEG-SEM; JEOL-JSM7001 F) at an accelerating voltage of 25 kV. The chemical composition was studied by energy dispersive X-ray analysis (SUTW-Sapphire) at an accelerating voltage of 15 kV. UV–Vis spectra were recorded in the interval range (200–800 nm) using a Multiskan SkyHigh Microplate Spectrophotometer (Thermo Scientific, Waltham, MA, USA). Fluorescence spectra were recorded using a Lumina fluorescence spectrometer (Thermo Scientific, Waltham, MA, USA) equipped with a 150 W xenon arc discharge lamp as the light source. The scanning speed was 600 nm/min; the integration time was 50 ms; the response time was 0.02 s. Both the excitation and emission slits were set to 20 nm, and both the emission and excitation filters were set to air.

2.3. Synthesis of the CdTe@MPA QD Nanoparticles

The aqueous soluble QDs were prepared according to Piloto et al. (2018) with minor modifications [16]. In a three-neck flask, $CdCl_2$ (6.59 mmol) was added to 60 mL of ultrapure water previously deaerated with nitrogen. Then, MPA (888 µL) was added to the cadmium solution in 60 mL ultrapure water, and the pH was adjusted to 11.5 by the dropwise addition of 1M sodium hydroxide. The resulting mixture was heated to 80° under constant nitrogen flow. Then, a solution of tellurium powder (0.299 mmol) with sodium borohydride (4.76 mmol) in 3 mL ultrapure water was prepared, heated to 60 °C, and added to the cadmium solution. The molar ratio (Cd^{2+}:Te^{2-}:MPA) was optimized to (1:0.05:1.5). The reaction mixture was refluxed at 120 °C for 30 min (Figure 1A). By extending the reflux time, the QDs' size increased with a shift of color, up to the red CdTe@MPA. Finally, the CdTe@MPA QDs were precipitated in ice in absolute ethanol (1:1) and centrifuged at 4000 rpm for 5 min. The resulting QDs were kept in a desiccator until they were dried. Finally, the different size QDs were ground and stored in a low humidity environment protected from light (Figure 1A).
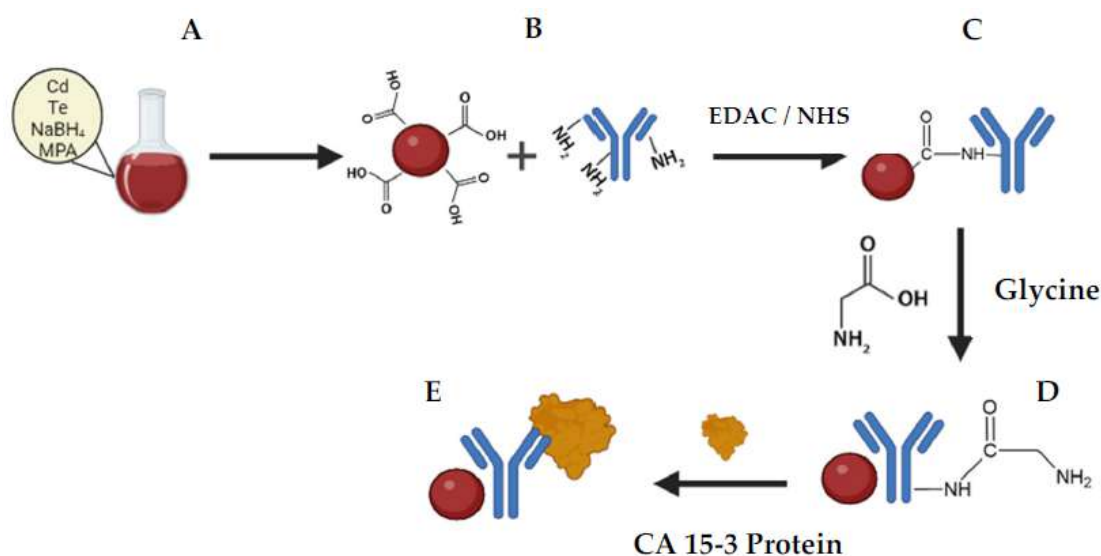
Figure 1. Schematic representation of the synthesis of the QD nanoparticles and preparation of the QD conjugates. (**A**) QD synthesis; (**B**) activation of carboxylic groups from QD; (**C**) covalent bond between the carboxylic groups from the nanoparticles and the amine groups from the antibodies, by the EDAC/NHS reaction; (**D**) blockage of unbound spaces; (**E**) binding of QD conjugates with the CA 15-3 protein.

2.4. Preparation of the QD Conjugates

For the preparation, 30 µL of a suspension of red-emitting CdTe@MPA QDs (5 mg/mL) prepared in PBS 10 mM at pH 7.4 was mixed with 25 µL EDAC (5.0×10^{-2} mg/mL) and 25 µL NHS (6.6×10^{-2} mg/mL) at a ratio of (1:1.33 eq.), followed by the addition of 20 µL of a solution of the CA 15-3 antibody (200 µg/mL) made in PBS 10 mM at pH 7.4 (Figure 1B). The final volume was adjusted to 500 µL with PBS 10 mM at pH 7.4 and incubated for 3 h at 30 °C with constant stirring. Next, 25 µL of glycine 0.01 M was added and incubated overnight at 4 °C (Figure 1C). Finally, the solution was purified using an Amicon Ultra centrifugal filter (Ultra-0.5) MWCO 50 kDa, to afford the correspondent suspension of the QD conjugates (Figure 1D).

The MPA cap on the surface of the QD was chosen to provide free carboxyl groups that could react and bind the molecules to the surface of the QD. In this way, the binding of the antibodies to the CdTe@MPA QDs was achieved by activation with EDAC/NHS. Overall, EDAC reacts with the carboxyl exposed on the surface of the QD groups to form an amine-reactive O-acyl isourea intermediate, which can be easily displaced by a nucleophilic attack of the primary amine groups of the antibody. The primary amine forms an amide bond with the carboxyl group, and an EDAC by-product is released as a soluble urea derivative. The intermediate O-acylisourea is unstable in aqueous solutions at physiological pH. If the intermediate does not react with an amine, it is hydrolyzed, re-forming the carboxyl groups and releasing an N-unsubstituted urea. To improve efficiency or to generate dry-stable (amine-reactive) intermediates, NHS is often added to EDAC couplings because it forms a more stable ester than the O-acylurea intermediate while allowing efficient conjugation with primary amines at physiological pH [29] (Figure 1 C). After conjugation of the QD nanoparticles with the antibodies, the remaining free sites were blocked with glycine (Figure 1D). Moreover, glycine reacts with the NHS esters and converts the original carboxylic acids into hydroxamic acids, which helps to stop the conjugation reaction [30]. The reaction was assessed using different times of the reaction (both reagents added together with no pre-reaction time with QD; 30 min pre-reaction with QD; 1 h pre-reaction with QD). The reaction conditions were chosen based on the amount of free nanoparticles filtered with the Amicon filters. Of all of these, the antibodies added after a 30 min pre-reaction of QD and EDAC/NHS showed the best results.

The prepared conjugate solution (200 µg/mL) was diluted, and two concentrations of antibodies were tested during conjugate assembly, 5 and 10 µg/mL, respectively. The assembly condition with 10 µg/mL of antibody was chosen because, under this condition, a better correlation was obtained between the fluorescence signal of the control solutions (the fluorescence intensity of the free QD nanoparticles in PBS 10 mM at pH 7.4) and the signal of the solutions of the QD conjugates in the presence of different concentrations of the target protein CA 15-3.

2.5. Detection and Quantification of the CA 15-3 Protein

All fluorescence measurements were performed under the same conditions. The excitation wavelength was set to 380 nm within an emission range from 550 to 730 nm. After each measurement, the fluorimeter temperature was assessed and cooled down up to 23–25 °C. The fluorescence signal was monitored in PBS buffer 10 mM at pH 7.4 and in 10-fold diluted human serum in PBS 10 mM at pH 7.4.

For the calibration assays, 10 µL of the CA 15-3 standard solutions (10–100) U/mL in PBS 10 mM at pH 7.4 was added to a suspension of the QD conjugates (10 µg/mL) in PBS 10 mM at pH 7.4, and the final volume was adjusted to 100 µL. Replicates of the suspensions were prepared (S/N = 3) and incubated for 10 min RT. The fluorescence signal was measured and plotted as a function of the total CA 15-3 protein concentration.

For the analysis of commercial human serum, pretreatment with Amicon filters (50kDa) was performed. The filtrate was discarded, and the remaining volume of supernatant was adjusted to the original serum volume. Subsequently, the human serum was diluted 10-fold in PBS 10 mM at pH 7.4, and several CA 15-3 protein standard solutions (10–100) U/mL were prepared in the diluted serum.

Replicates of the suspensions were prepared (S/N = 3) following the protocol previously described. The limit of detection (LOD) was calculated using the following formula:

$$LOD = (3\delta \text{ (lowest concentration))}/\text{(curve slope)}$$

where δ represents the standard deviation obtained for the lowest concentration of CA 15-3 [31].

2.6. Selectivity Studies

Three interfering species detected in human serum were tested using competition assays, and selectivity was examined for each interfering species individually. All assays were performed in triplicate (S/N = 3). Solutions of the interfering species were prepared in the pretreated 10-fold diluted human serum in PBS 10 mM at pH 7.4 to a final concentration of BSA (1 mg/mL), CEA (3 ng/mL), and CA 125 (30 U/mL). The solutions were incubated as previously described, and the percentage of interference was determined by comparison with the fluorescent signal obtained with a 30 U/mL standard solution of CA 15-3 prepared in the same medium.

2.7. Reproducibility Studies

Biosensor reproducibility was evaluated with three concentrations of CA 15-3 in 10-fold diluted human serum in PBS 10 mM at pH 7.4, with the diluted human serum serving as a blank. All assays were performed in triplicate, at room temperature, and the respective RSD values were calculated. The average recovery and RSD values are shown in Table 1. Recovery values were determined using the following formula:

$$\% \text{ recovery} = (\text{CA 15-3 Theorical}/\text{CA 15-3 Experimental}) \times 100.$$

Table 1. Evaluation of the reproducibility of the sensor by testing it with commercial serum spiked with the CA 15-3 protein (n = 3).

Sample	Intensity (Counts)	Recovery (%)	RSD (%)
10 U/mL	9169.73	99.66	0.28
30 U/mL	8094.8	99.93	0.61
75 U/mL	5726.04	100.61	1.56

3. Results and Discussion

3.1. Characterization of the QD Nanoparticles

3.1.1. Optical Characterization of the QD Nanoparticles

The absorption spectra of QD nanoparticles suspended in PBS 10 mM at pH 7.4 are shown in Figure 2. During synthesis, the size growth of the QDs was observed over time under a UV lamp at 365 nm (Figure 2A). As expected, extending the reflux time during the synthesis of QD nanoparticles resulted in bathochromic shifts in the emission spectra and an increase in size, as demonstrated previously by Piloto et al. [16]. The diameter of the synthesized CdTe@MPA QDs was calculated using the following equation [32]:

$$D = (9.8127 \times 10^{-7})\, \lambda^3 - (1.7147 \times 10^{-3})\, \lambda^2 + (1.0064)\, \lambda - 194.84$$

where D is the diameter of the nanoparticles (nm) and λ is the wavelength of maximum absorption, as shown in Figure 2B. The maximum absorption for the red-emitting QD nanoparticles was set at 580 nm, since this corresponds to the inflection point of the curve at which the red QD absorb energy. According to the above equation, the theoretical diameter of the red-emitting QDs is 3.50 nm.
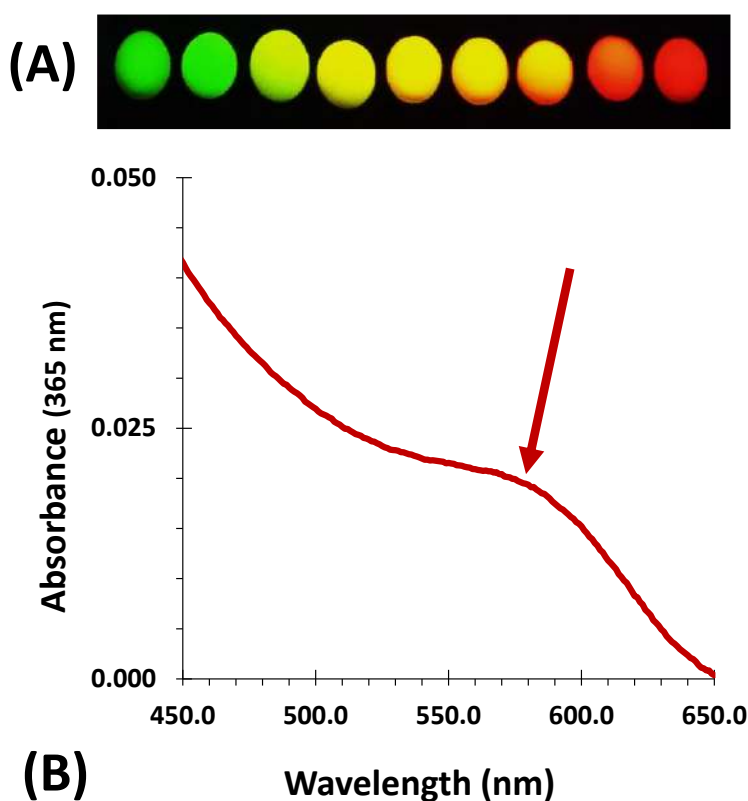

Figure 2. (**A**) Crude solutions of the CdTe@MPA QDs taken along their synthesis and photographed under a 365 nm UV lamp. (**B**) UV–Vis spectrum of the red-emitting QDs with the maximum wavelength at 580 nm was selected as the maximum absorption wavelength of the red-emitting QDs.

A solution of red-emitting QD nanoparticles (1 mg/mL) was analyzed by fluorescence spectroscopy. The excitation and emission spectra for two wavelengths are shown in Figure S1. The emission profiles of QD nanoparticles have the shape of Gaussian functions, and the wavelength of the peaks varies as a function of particle size. A smaller half-wavelength width (FWHM) is associated with more purely colored QDs and higher efficiencies [33]. In addition, the excitation wavelength of 380 nm was chosen because it gave a complete emission curve compared to using higher excitation wavelengths The curve exhibited an emission maximum at 633 nm and an FWHM of 60.9 nm.

3.1.2. SEM and TEM Analysis

TEM images show that the red-emitting CdTe@MPA QDs are arranged as spherical aggregates with a size of less than 5 nm (Figure 3A). This is confirmed by the images from SEM, where the nanoparticles have variable diameters of up to 56 nm. This behavior was to be expected if the nanoparticles tend to aggregate in the solid state, and sonication is required to avoid this behavior.
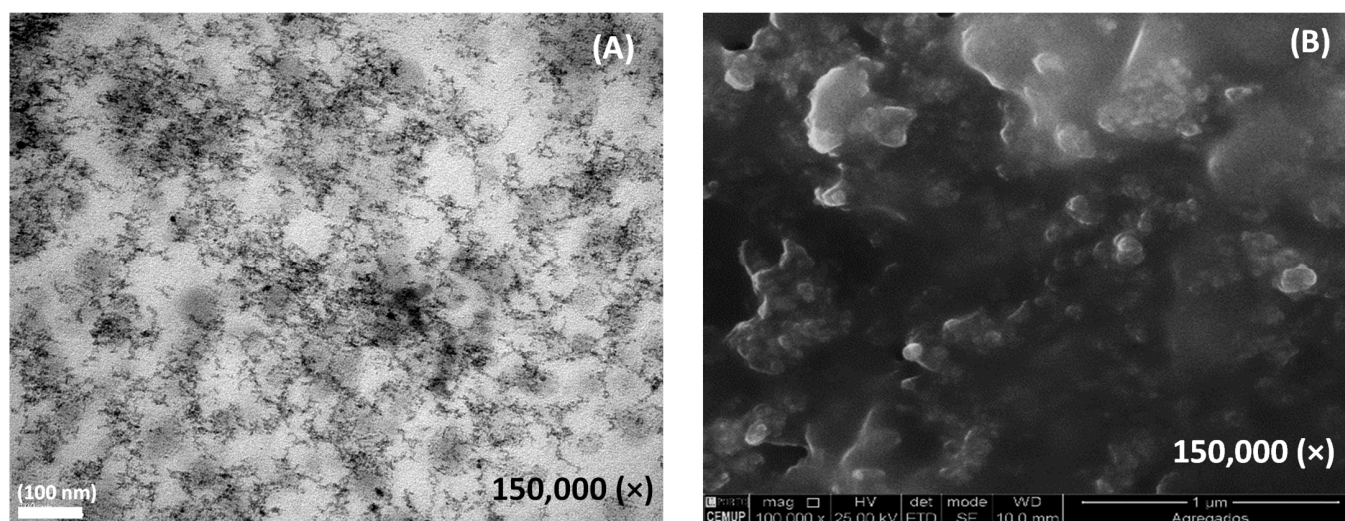

Figure 3. (**A**) TEM images of red-emitting CdTe@MPA QDs resuspended in ultrapure water; (**B**) SEM image of red-emitting CdTe@MPA QDs resuspended in ultrapure water.

SEM images of the CdTe@MPA QDs can be seen in Figure 3B. It can be observed that the nanoparticles agglomerated into clusters up to 56 nm in size. These images were taken after resuspension of both materials in ultrapure water.

The EDS analysis evidences the sulfur, carbon, and oxygen elements from the mercaptopropionic acid used to cap the QD nanoparticles—Figure S2. The presence of cadmium and telluride elements from the metallic core of the nanoparticles and the presence of sodium from the sodium borohydride used as a reducing agent are also detectable.

3.1.3. FTIR

The chemical conjugation of the CA 15-3 antibody with the red-emitting CdTe@MPA QDs was characterized by FTIR spectroscopy. In Figure 4 are shown the spectra of the CdTe@MPA QDs (red) (i), of the CA 15-3 antibody (purple) (ii), and of the CdTe@MPA conjugates (red) (iii).

The two peaks observed in the CdTe@MPA QDs at 1552.08 cm^{-1} and 1392.71 cm^{-1} correspond to the asymmetric and symmetric stretching, respectively, of the carboxylic acids of the QD nanoparticles. Moreover, the band at 3300 cm^{-1} is due to the OH stretching bond. Upon conjugation of the antibody to the surface of the QDs, a wide band at 3302.08 cm^{-1} is visible, which is responsible for the N-H and O-H stretchings of the amine and carboxylic acids of the protein, respectively. The peak at 1648.69 cm^{-1} represents

the N-H bending vibrations of the amino acid residues. The two bands at 2935.88 cm^{-1} and 2880.78 cm^{-1} belong to the carbon-hydrogen (CH$_2$) vibrational peaks. The attenuated asymmetric stretching band in the spectrum of the conjugated QDs is derived from the MPA capping of the QD nanoparticles.
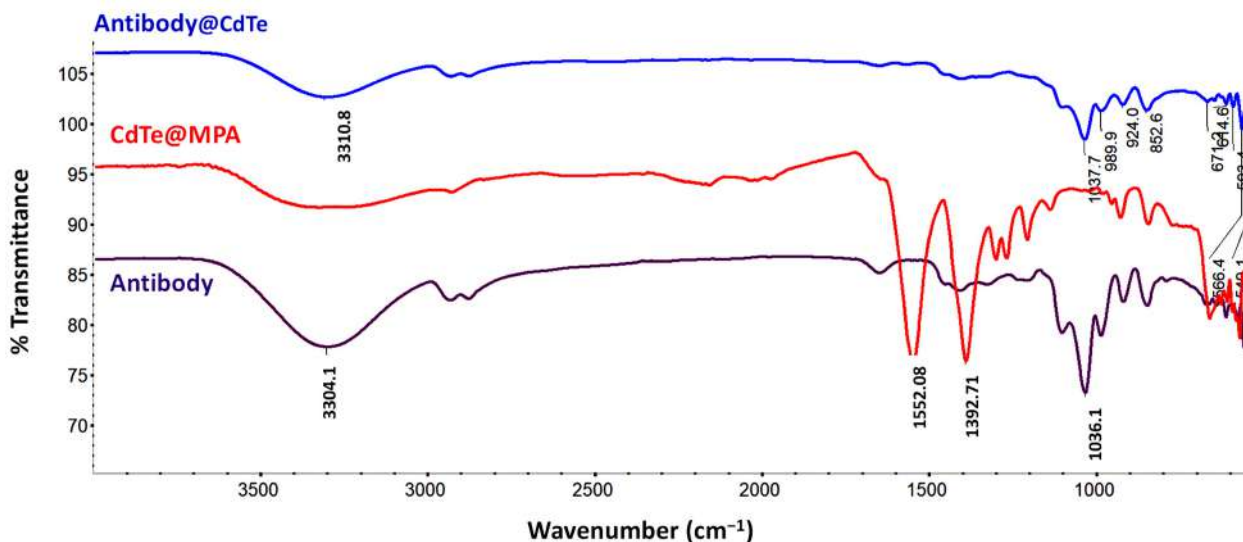

Figure 4. FTIR spectra of the CdTe@MPA QDs (red) (i), of the CA 15-3 antibody (blue) (ii), and of the CdTe@MPA conjugates (purple) (iii).

3.2. Stability of the QDs Conjugates

Fluorescence spectroscopy was used to evaluate the stability of the QD conjugates for 10 days (Figure 5). After the CdTe@MPA QDs were modified with the antibodies, a prominent decrease in the fluorescence peak intensity was observed, as the attachment of the biomolecule increases the size of the particle, leading to a lower confinement energy [3,34].
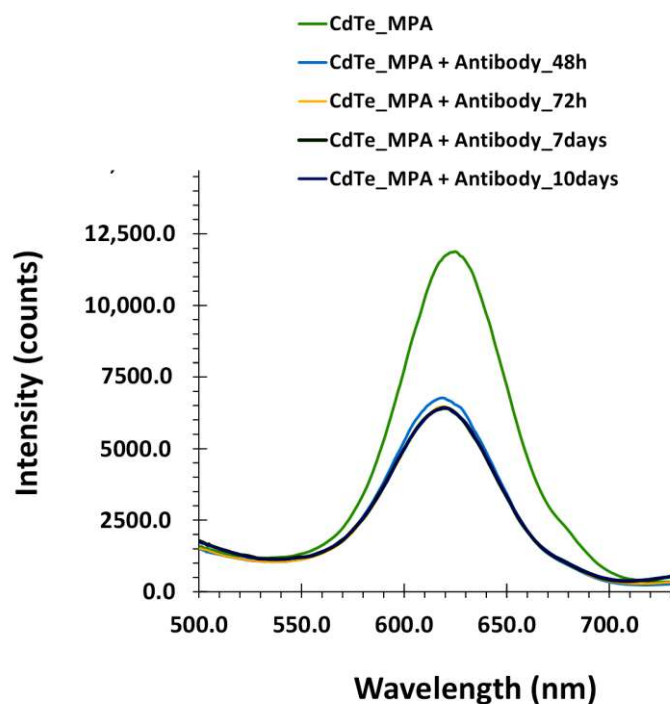

Figure 5. CdTe@MPA QD and their conjugation with CA 15-3 antibody emission spectra using a photomultiplier tube voltage of 400 PMT and an excitation wavelength of 380 nm (n = 3).

The QD conjugates cause a hypsochromic shift (to lower wavelengths) in the emission spectra, along with a decrease in fluorescence intensity. The QD conjugates were monitored over time.

The first measurement was performed 48 h after the preparation of the system. After 72 h, the sample showed an intensity loss of 3.86%. This value remained almost the same during the stability study, varying from a signal loss of 0.13% after 7 days to a loss of 0.76% after 10 days. From these results, it can be concluded that the solutions of QD conjugates require 72 h after their preparation to stabilize, with the initial signal remaining stable for up to 10 days.

3.3. Calibration Curve

The ability of QD conjugates to show a linear response in the presence of the target protein CA 15-3 in a spiked buffer was investigated by fluorescence spectroscopy (Figure S3). The emission wavelength was set at 624.2 nm because the calibration curves showed a higher slope at this wavelength, which improved the sensitivity of this method.

During the calibrations of QD conjugates with increasing concentrations of CA 15-3 protein standards prepared in PBS 10 mM at pH 7.4, the fluorescence intensity of QD conjugates decreased, as shown in Figure S3. From these results, we concluded that recognition of the CA 15-3 protein attenuates the QDs' fluorescence. Overall, we can conclude that the QD conjugates were able to discriminate a sample from 0.09 U/mL to 0.45 U/mL and limit of detection of 0.027 U/mL, and the low error bars show the reproducibility of the CA 15-3 biosensor developed in this work.

Next, the device was tested in 10-fold diluted spiked human serum in PBS 10 mM at pH 7.4. Initially, the calibrations were performed in undiluted human serum, but the highly concentrated and complex human serum matrix promoted fluorescence attenuation of the red-emitting QDs, resulting in a conditioned response of the CA 15-3 biosensor. For this reason, human serum was first filtered to remove positively charged salts that affect the fluorescence of the QDs and, consequently, the stability of the biosensor. This pretreatment also removed smaller molecules such as glucose and smaller proteins. The correspondent fluorescence emission spectra are presented in Figure 6.
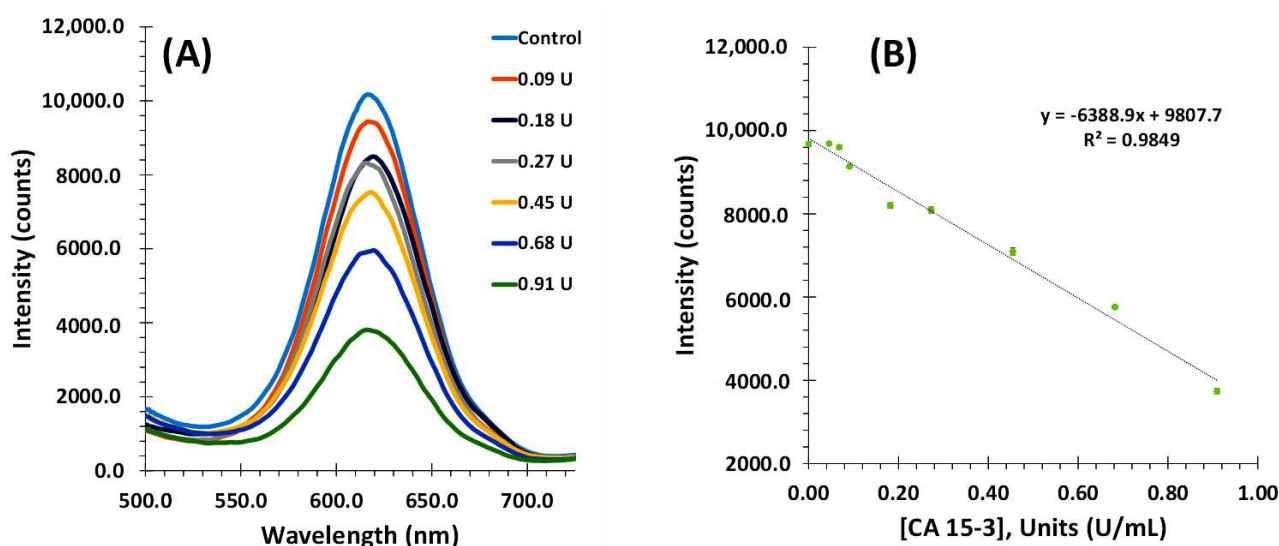

Figure 6. (**A**) Emission spectra of QD conjugates during protein recognition. (**B**) The calibration curve was performed in 10-fold diluted commercial human serum. The analysis was conducted using a photomultiplier tube voltage of 410 PMT and an excitation wavelength of 380 nm (n = 3).

Overall, fluorescence emission decreased in the presence of the target and provided a linear regression with a correlation coefficient greater than 0.98. The developed CA 15-3 biosensor showed a linear response between 0.09 U/mL and 0.91 U/mL.

The threshold value for normal individuals is 25–30 U/mL. In this way, our method was able to distinguish spiked from non-spiked samples in an artificial human serum, with a detection limit of 0.027 U/mL and a lower limit of the linear range of 0.09 U/mL. The LOD of this research shows a 10-times lower LOD when compared to available automated kits, namely the Access 2 (0.5 U/mL) or AxSYM (0.3 U/mL) [34]—Table 2.

Table 2. Comparison of techniques described in the literature for CA 15-3 measurement.

Technique	Limit of Detection	References
Access 2—Automated Kit	0.5 U/mL	[35]
ARCHITECT i2000SR—Automated Kit	0.5 U/mL	[35]
AxSYM—Automated Kit	0.3 U/mL	[35]
Electrochemical device	0.01–0.2 U/mL	[36]
Photoluminescence	0.002 U/mL	[37]
Fluorescence	0.027 U/mL	Current Study

3.4. Selectivity Studies

Selectivity studies were conducted in this work to evaluate how serum species could possibly interfere with the biosensor response to the target protein, CA 15-3. As the human serum samples were pre-treated first, only species with high molecular weights were considered. The results are presented in Figure 7.
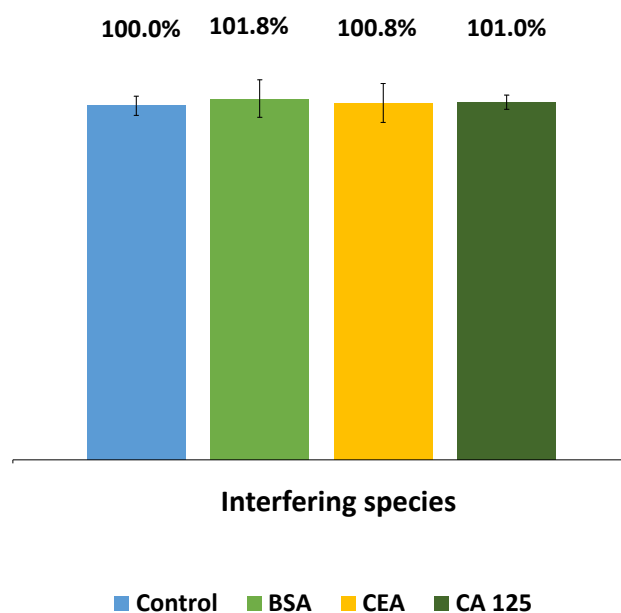

Figure 7. Selectivity study for the CA 15-3 biosensor. The interfering species used were BSA (1 mg/mL), CEA protein (3 ng/mL), and CA 125 (30 U/mL). The samples with 30 U/mL of CA 15-3 were all diluted as for the serum tests (n = 3).

For the selectivity study, BSA (1 mg/mL) was selected as an interfering agent because of its high abundance in serum. In addition, CEA and CA 125 were also selected because these proteins are normally present in serum in various cancers, particularly breast cancer. These proteins were evaluated using normal serum cut-off values, specifically the CEA protein at (3 ng/mL) and the CA 125 protein at (30 U/mL).

The presence of the CEA and CA 125 proteins represented a 1% deviation in the response of the CA 15-3 biosensor. The larger deviation occurred with the BSA protein (2%). Overall, the presence of interfering species did not result in significant deviations in the biosensor response. These results suggest that the biosensor can provide a selective response based primarily on the concentration of the CA 15-3 target.

3.5. Sample Analysis

The practicability of the CA 15-3 biosensor was evaluated by testing it with commercially diluted human serum containing known concentrations of the CA 15-3 protein. Tests were conducted with three distinct conditions. These included: (i) testing with the cut-off value for CA 15-3 (30 U/mL), (ii) its upper limit concentration (10 U/mL), and (iii) using a higher concentration of the CA 15-3 protein (75 U/mL). The readings were performed in triplicate, and the concentration of each sample was calculated based on the fluorescence intensity measured in the calibration curve obtained with the 10-fold diluted human serum. In order for the solution to have the same basal intensity as the batch used in the serum calibration, the PMT that excites the sample was higher (418 PMT).

In Table 1 are presented the recovery results of CA 15-3 and the corresponding RSD% values.

The recovery rate of CA 15-3 were ~99.66% for 10 U/mL, ~99.93% for 30 U/mL, and ~100.61% for 75 U/mL. The RSD% values ranged from 0.28 to 1.56, being higher for the 75 U/mL sample. With the high recovery values and small RSD values, the reproducibility of the device is demonstrated, suggesting it is practical for measuring the CA15-3 protein in real human serum samples.

4. Conclusions

Fluorescent biosensing devices are extensively studied for point-of-care purposes due to their high sensitivity allied with their affordable price and easy and fast reading. This work presented a novel QD-based biosensor to detect and quantify the CA 15-3 protein in human serum samples. The detection was achieved by direct conjugation of red-emitting QD nanoparticles with the CA 15-3 antibody. The biosensor provided a linear correlation between the concentration of CA 15-3 in the sample and its fluorescence intensity, both in buffer and in human serum, with a limit of detection of 0.027 U/mL in 10-fold diluted human serum. Furthermore, the biosensor showed high recovery ratios when used with spiked human serum samples, representing an affordable and simple means of measuring analytes of interest.

Conflicts of Interest: The authors declare no conflict of interest.

References

1. Cotta, M.A. Quantum Dots and Their Applications: What Lies Ahead? *ACS Appl. Nano Mater.* **2020**, *3*, 4920–4924. [CrossRef]
2. Maxwell, T.; Nogueira Campos, M.G.; Smith, S.; Doomra, M.; Thwin, Z.; Santra, S. Quantum Dots. In *Micro and Nano Technologies*; Chung, E.J., Leon, L., Rinaldi, C., Eds.; Elsevier: Amsterdam, The Netherlands, 2020; Chapter 15; pp. 243–265, ISBN 978-0-12-816662-8.
3. Sumanth Kumar, D.; Jai Kumar, B.; Mahesh, H.M. Quantum Nanostructures (QDs): An Overview. In *Micro and Nano Technologies*; Mohan Bhagyaraj, S., Oluwafemi, O.S., Kalarikkal, N., Thomas, S., Eds.; Woodhead Publishing: Sawston, UK, 2018; Chapter 3; pp. 59–88, ISBN 978-0-08-101975-7.
4. De la Calle, I.; Romero-Rivas, V. The Role of Nanomaterials in Analytical Chemistry: Trace Metal Analysis. In *Micro and Nano Technologies*; Mohan Bhagyaraj, S., Oluwafemi, O.S., Kalarikkal, N., Thomas, S., Eds.; Woodhead Publishing: Sawston, UK, 2018; Chapter 9; pp. 251–301, ISBN 978-0-08-101971-9.
5. Kargozar, S.; Hoseini, S.J.; Milan, P.B.; Hooshmand, S.; Kim, H.-W.; Mozafari, M. Quantum Dots: A Review from Concept to Clinic. *Biotechnol. J.* **2020**, *15*, e2000117. [CrossRef] [PubMed]
6. Liang, Z.; Khawar, M.B.; Liang, J.; Sun, H. Bio-Conjugated Quantum Dots for Cancer Research: Detection and Imaging. *Front. Oncol.* **2021**, *11*, 749970. [CrossRef] [PubMed]
7. Tandale, P.; Choudhary, N.; Singh, J.; Sharma, A.; Shukla, A.; Sriram, P.; Soni, U.; Singla, N.; Barnwal, R.P.; Singh, G.; et al. Fluorescent Quantum Dots: An Insight on Synthesis and Potential Biological Application as Drug Carrier in Cancer. *Biochem. Biophys. Rep.* **2021**, *26*, 100962. [CrossRef] [PubMed]
8. Pleskova, S.; Mikheeva, E.; Gornostaeva, E. Using of Quantum Dots in Biology and Medicine. *Adv. Exp. Med. Biol.* **2018**, *1048*, 323–334. [CrossRef]
9. Lu, H.; Li, W.; Dong, H.; Wei, M. Graphene Quantum Dots for Optical Bioimaging. *Small* **2019**, *15*, 1902136. [CrossRef] [PubMed]
10. Kadim, A.M. Applications of Cadmium Telluride (CdTe) in Nanotechnology. In *Nanomaterials-Toxicity, Human Health and Environment*; IntechOpen: London, UK, 2020; pp. 1–11. [CrossRef]
11. Akbari, M.; Rahimi-Nasrabadi, M.; Pourmasud, S.; Eghbali-Arani, M.; Banafshe, H.R.; Ahmadi, F.; Ganjali, M.R.; Sobhani nasab, A. CdTe Quantum Dots Prepared Using Herbal Species and Microorganisms and Their Anti-Cancer, Drug Delivery and Antibacterial Applications; a Review. *Ceram. Int.* **2020**, *46*, 9979–9989. [CrossRef]
12. Ebrahim, S.; Reda, M.; Hussien, A.; Zayed, D. CdTe Quantum Dots as a Novel Biosensor for Serratia Marcescens and Lipopolysaccharide. *Spectrochim. Acta-Part A Mol. Biomol. Spectrosc.* **2015**, *150*, 212–219. [CrossRef]
13. Zhu, L.; Hao, H.; Ding, C.; Gan, H.; Jiang, S.; Zhang, G.; Bi, J.; Yan, S.; Hou, H. A Novel Photoelectrochemical Aptamer Sensor Based on Cdte Quantum Dots Enhancement and Exonuclease I-Assisted Signal Amplification for Listeria Monocytogenes Detection. *Foods* **2021**, *10*, 2896. [CrossRef]
14. Nguyen, T.H.; Ung, T.D.T.; Vu, T.H.; Tran, T.K.C.; Dong, V.Q.; Dinh, D.K.; Nguyen, Q.L. Fluorescence Biosensor Based on CdTe Quantum Dots for Specific Detection of H5N1 Avian Influenza Virus. *Adv. Nat. Sci. Nanosci. Nanotechnol.* **2012**, *3*, 035014. [CrossRef]
15. Li, X.; Zhou, Y.; Zheng, Z.; Yue, X.; Dai, Z.; Liu, S.; Tang, Z. Glucose Biosensor Based on Nanocomposite Films of CdTe Quantum Dots and Glucose Oxidase. *Langmuir* **2009**, *25*, 6580–6586. [CrossRef] [PubMed]
16. Piloto, A.M.; Ribeiro, D.S.M.; Rodrigues, S.S.M.; Santos, C.; Santos, J.L.M.; Sales, M.G.F. Plastic Antibodies Tailored on Quantum Dots for an Optical Detection of Myoglobin down to the Femtomolar Range. *Sci. Rep.* **2018**, *8*, 4944. [CrossRef] [PubMed]
17. WHO Cancer. Available online: https://www.who.int/health-topics/cancer (accessed on 1 May 2022).
18. Lebron-Zapata, L.; Jochelson, M.S. Overview of Breast Cancer Screening and Diagnosis. *PET Clin.* **2018**, *13*, 301–323. [CrossRef] [PubMed]
19. Duffy, M.J.; Walsh, S.; McDermott, E.W.; Crown, J. *Biomarkers in Breast Cancer: Where Are We and Where Are We Going?* 1st ed.; Elsevier Inc.: Amsterdam, The Netherlands, 2015; Volume 71, ISBN 9780128022566.
20. Aydin, S. A Short History, Principles, and Types of ELISA, and Our Laboratory Experience with Peptide/Protein Analyses Using ELISA. *Peptides* **2015**, *72*, 4–15. [CrossRef]
21. Issaq, H.J.; Veenstra, T.D. *Analytical Methods and Biomarker Validation*; Elsevier: Amsterdam, The Netherlands, 2013; ISBN 9780123944467.
22. Patel, S.; Nanda, R.; Sahoo, S.; Mohapatra, E. Biosensors in Health Care: The Milestones Achieved in Their Development towards Lab-on-Chip-Analysis. *Biochem. Res. Int.* **2016**, *2016*, 3130469. [CrossRef]
23. Fakhari, A.; Gharepapagh, E.; Dabiri, S.; Fakhari, A.; Gharepapagh, E.; Dabiri, S.; Gilani, N. Correlation of Cancer Antigen 15-3 (CA15-3) Serum Level and Bony Metastases in Breast Cancer Patients. *Med. J. Islam. Repub. Iran* **2019**, *33*, 142. [CrossRef]
24. Vengesai, A.; Midzi, H.; Kasambala, M.; Mutandadzi, H.; Mduluza-Jokonya, T.L.; Rusakaniko, S.; Mutapi, F.; Naicker, T.; Mduluza, T. A systematic and meta-analysis review on the diagnostic accuracy of antibodies in the serological diagnosis of COVID-19. *Syst. Rev.* **2021**, *10*, 155. [CrossRef]
25. Ribeiro, J.A.; Pereira, C.M.; Silva, A.F.; Sales, M.G.F. Disposable Electrochemical Detection of Breast Cancer Tumour Marker CA 15-3 Using Poly(Toluidine Blue) as Imprinted Polymer Receptor. *Biosens. Bioelectron.* **2018**, *109*, 246–254. [CrossRef]

26. Oktaviyanti, I.K.; Ali, D.S.; Awadh, S.A.; Opulencia, M.J.C.; Yusupov, S.; Dias, R.; Alsaikhan, F.; Mohammed, M.M.; Sharma, H.; Mustafa, Y.F.; et al. Recent Advances on Applications of Immunosensing Systems Based on Nanomaterials for CA15-3 Breast Cancer Biomarker Detection. *Anal. Bioanal. Chem.* **2022**, 1–12. [CrossRef]

27. Zubair, M.; Wang, S.; Ali, N. Advanced Approaches to Breast Cancer Classification and Diagnosis. *Front. Pharmacol.* **2021**, *11*, 632079. [CrossRef]

28. Bahari, D.; Babamiri, B.; Salimi, A. Ultrasensitive Molecularly Imprinted Fluorescence Sensor for Simultaneous Determination of CA125 and CA15–3 in Human Serum and OVCAR-3 and MCF-7 Cells Lines Using Cd and Ni Nanoclusters as New Emitters. *Anal. Bioanal. Chem.* **2021**, *413*, 4049–4061. [CrossRef] [PubMed]

29. Moreira, F.T.C.; Sharma, S.; Dutra, R.A.F.; Noronha, J.P.C.; Cass, A.E.G.; Sales, M.G.F. Smart Plastic Antibody Material (SPAM) Tailored on Disposable Screen Printed Electrodes for Protein Recognition: Application to Myoglobin Detection. *Biosens. Bioelectron.* **2013**, *45*, 237–244. [CrossRef] [PubMed]

30. Thermo Fisher Scientific. *NHS and Sulfo-NHS Instructions*; Thermo Fisher Scientific Inc.: Waltham, MA, USA, 2011.

31. Virgilio, A.; Silva, A.B.S.; Nogueira, A.R.A.; Nóbrega, J.A.; Donati, G.L. Calculating Limits of Detection and Defining Working Ranges for Multi-Signal Calibration Methods. *J. Anal. At. Spectrom.* **2020**, *35*, 1614–1620. [CrossRef]

32. Yu, W.W.; Qu, L.; Guo, W.; Peng, X. Experimental Determination of the Extinction Coefficient of CdTe, CdSe, and CdS Nanocrystals. *Chem. Mater.* **2003**, *15*, 2854–2860. [CrossRef]

33. Dai, X.; Deng, Y.; Peng, X.; Jin, Y. Quantum-Dot Light-Emitting Diodes for Large-Area Displays: Towards the Dawn of Commercialization. *Adv. Mater.* **2017**, *29*, 1607022. [CrossRef]

34. Zhirnov, V.V.; Cavin, R.K. Basic Physics of ICT. In *Micro and Nano Technologies*; Zhirnov, V.V., Cavin, R.K., Eds.; William Andrew Publishing: Oxford, UK, 2015; Chapter 2; pp. 19–49, ISBN 978-0-323-31302-5.

35. Slev, P.R.; Rawlins, M.L.; Roberts, W.L. Performance Characteristics of Seven Automated CA 15-3 Assays. *Am. J. Clin. Pathol.* **2006**, *125*, 752–757. [CrossRef]

36. Altintas, Z.; Kallempudi, S.S.; Gurbuz, Y. Gold nanoparticle modified capacitive sensor platform for multiple marker detection. *Talanta* **2014**, *118*, 270–276. [CrossRef]

37. Elakkiya, V.; Menon, M.P.; Nataraj, D.; Biji, P.; Selvakumar, R. Optical detection of CA 15.3 breast cancer antigen using CdS quantum dot. *IET Nanobiotechnol.* **2017**, *11*, 268–276. [CrossRef]